Appl. Phys. B 63, 599–604 (1996)

Applied Physics B Lasers and Optics

Holographic scattering lines observed with photorefractive $BaTiO_3$

J. Neumann, G. Jäkel, E. Krätzig

Universität Osnabrück, Fachbereich Physik, D-49069 Osnabrück, Germany
(Fax: + 49-541/969-2670, E-mail: JENS.NEUMANN@Physik.Uni-Osnabrueck.de)

Received: 25 January 1996/accepted: 24 April 1996

Abstract. We investigate holographic scattering processes in $BaTiO_3$ pumped by two coherent copropagating waves. Four lines are observed on a screen behind the sample. The experimental results are well described by a model taking into account parametric mixing of four copropagating waves and limitations of optically induced space charge fields because of the finite trap density.

PACS: 42.40; 42.65; 42.70

In the last decade many interesting light-induced scattering phenomena have been observed in photorefractive crystals [1–8]. In principle all nonlinear scattering nearly degenerate in frequency results from the same effect: A variety of "noisy" volume phase grating are recorded by incident light waves and waves scattered from volume or surface imperfections of the crystal. Subsequently, the scattered light is amplified because of direct coupling of two beams by a shifted grating [9] or as a result of parametric mixing of more than two waves [10, 11]. It was shown [7, 8] that two types of parametric processes occur, *A* and *B*, which are defined by the phase matching conditions

$$\mathbf{k}_{p1} + \mathbf{k}_{p2} = \mathbf{k}_{s1} + \mathbf{k}_{s2}, \tag{1a}$$

$$\mathbf{k}_{p1} - \mathbf{k}_{p2} = \mathbf{k}_{s1} - \mathbf{k}_{s2}. \tag{1b}$$

Here $\mathbf{k}_{p1}$, $\mathbf{k}_{p2}$ denote the wave vectors of the two pump waves and $\mathbf{k}_{s1}$ and $\mathbf{k}_{s2}$, the wave vectors of a pair of parametrically coupled scattered waves. The gain factor for the scattering critically depends on these phase-matching conditions. As a result, the scattered light propagates in limited angular windows with characteristic intensity distributions. For copropagating pump waves the *A*-processes manifest themselves in scattering rings and the *B*-processes in unclosed, slightly curved lines on a viewing screen behind the sample. In uniaxial crystals there exist two types of optical eigenmodes different in polarization, ordinary (o) and extraordinary (e) waves. Applying this fact to (1), nine different elementary *A*- and 10 *B*-processes are obtained [12].

Of particular interest are scattering effects in photorefractive $BaTiO_3$ because of its very large electrooptic coefficients. Here different scattering rings [1–5] and lines [6, 13] have been discovered. In [13] we reported on a *B*-process in $BaTiO_3$ pumped by two ordinary copropagating waves which yields four scattering lines on a screen behind the sample. If counterpropagating pump waves meeting the same phase-matching conditions are introduced, too, mirrorless oscillation occurs.

In the present paper we perform an extended analysis of this parametric process. Additionally we consider extraordinarily polarized pump waves. First we describe the basic experimental observations and then we present a model of this nonlinear mixing of coherent light waves. The scattering geometry and the steady-state gain factor are investigated in detail. Finally we report on further experiments supporting our model.

1 Basic experimental observations

We use single domain $BaTiO_3$ crystals grown in the crystal-growth laboratory of the physics department of the University of Osnabrück. Most experiments are performed with a sample of dimensions 4.2 mm × 5.0 mm × 4.8 mm ($a \times b \times c$) cut along the principal crystal axes and containing an effective trap number $N_{eff} = 4 \times 10^{22}$ m^{-3}, as determined by beam-coupling measurements (see, e.g., [14]).

The experimental arrangement for our investigations is shown schematically in Fig. 1. Two light beams of an Ar^+-ion laser (TEM_{00} mode, wavelength $\lambda = 514.5$ nm, intensity $I = 7000$ W/m^2) impinge upon a $BaTiO_3$ crystal symmetrically. The unexpanded pump beams form an angle of $2\theta_p$ (in air) in the plane of incidence, which is chosen to be perpendicular to the **c**-axis of the sample. A phase retarder ($\lambda/2$ plate) is used to obtain ordinary or extraordinary polarization of the pump waves. The scattering patterns are observed with the help of a screen placed about 1 m behind the crystal.

At the very beginning of exposure only the two spots marking the positions of the pump waves are visible on

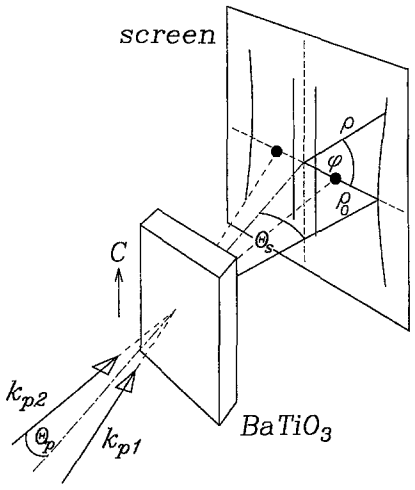

Fig. 1. Experimental arrangement; $\mathbf{k}_{p1}$ and $\mathbf{k}_{p2}$ denote the wave vectors of the pump waves, ρ and ϕ the polar coordinates on the screen, θ_s is the scattering angle and θ_p the pump angle

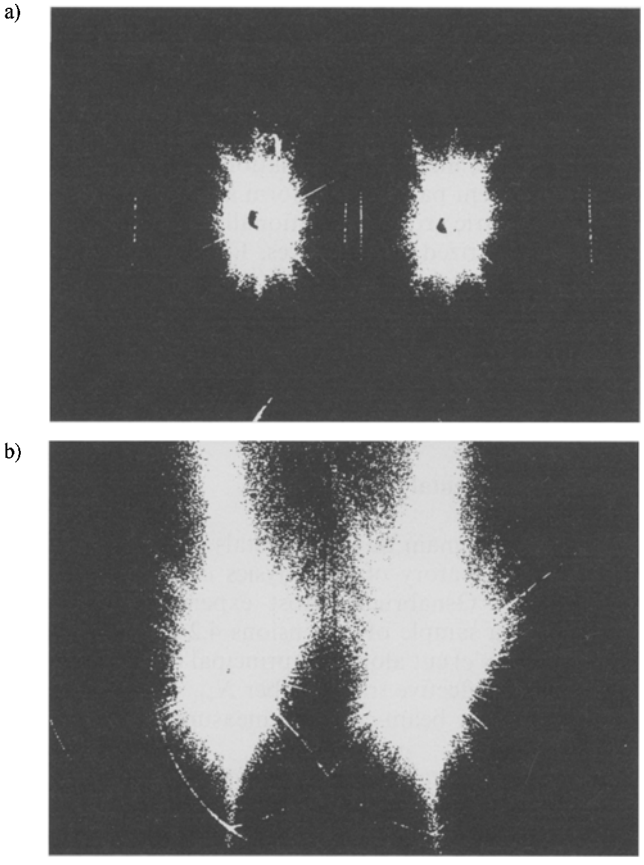

Fig. 2a, b. Intensity distribution on a screen behind the crystal for (**a**) ordinarily and (**b**) extraordinarily polarized pump beams

the screen. Then, during continuous illumination with ordinarily polarized pump waves, we observe the development of four scattering lines (Fig. 2a). The light scattered into the outer lines has also ordinary polarization, whereas the light scattered into the inner lines is extraordinarily

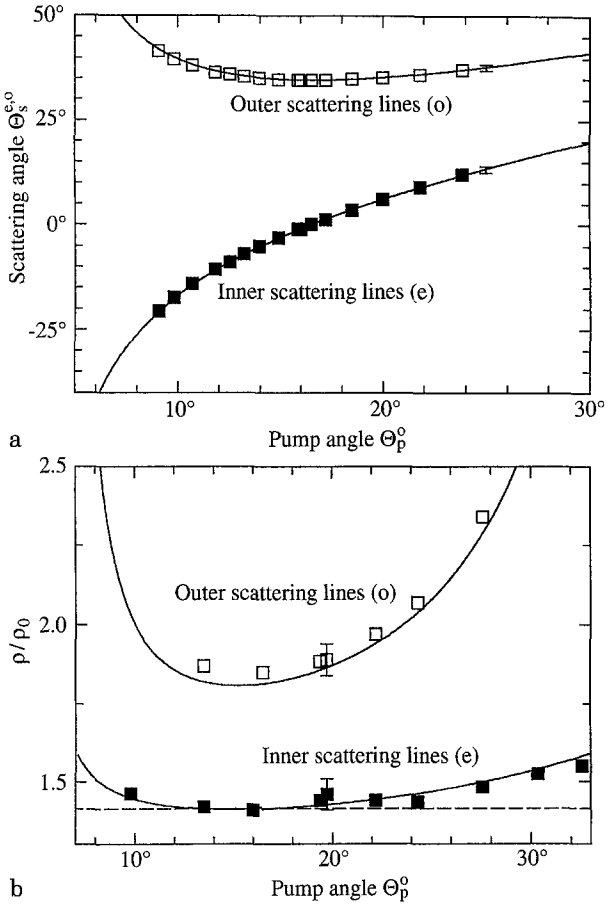

Fig. 3a, b. Scattering angles θ_s^e and θ_s^o of the inner and outer scattering lines in the plane of incidence vs pump angle θ_p (all angles in air). (**b**) Deviations ρ/ρ_0 from straight lines at an azimuth angle $\phi = 45°$ as a function of pump angle θ_p. The full lines are calculated (no free parameter) from (2) and (3), and the squares are measured values. For comparison the dashed line showing the relation $\rho/\rho_0 = 1/\cos 45°$ is also included

polarized. When we change the polarization of the pump waves to extraordinary polarization, we observe dark inner lines inside the scattered noise and very weak (barely visible), extraordinarily polarized outer lines (Fig. 2b). In addition, scattering rings are found which will not be considered in the following. For both polarizations the intensity of the scattering pattern is symmetric with respect to the plane defined by the **c**-axis and the bisector of the two pump waves.

The measured scattering angles θ_s^e and θ_s^o of the inner and outer lines in the plane of incidence are shown in Fig. 3a as a function of the pump angle θ_p. The solid curves represent the calculated dependences (see Sect. 2). The scattered lines on the screen are not perfectly parallel straight lines. The deviation can be expressed by the quantity ρ/ρ_0 as a function of the pump angle θ_p and the azimuth angle ϕ (see Fig. 1). Fig. 3b represents the measured dependence of ρ/ρ_0 at $\phi = 45°$ fitting well to the calculated dependences (Sect. 2). Both, scattering angles and the deviation from straight lines, are the same for ordinarily and extraordinarily polarized pump beams.

2 Theory

2.1 Description of the model

For $BaTiO_3$ we can neglect grating recording via the photovoltaic effect in comparison to recording via diffusion. The gratings are written by pairs consisting of two waves with the same polarization and the gratings are phase-shifted by $\pi/2$ with respect to the interference fringes. Furthermore, electrooptic tensor coefficients involved in anisotropic diffraction ($r_{232} = r_{131} \simeq$ 1300 pm/V) are much larger than that for isotropic diffraction ($r_{113} = 8$ pm/V and $r_{333} \simeq 103$ pm/V) [15]. For this reason mainly anisotropic diffraction is of importance.

We propose the phase matching conditions (1b) and the wave vector diagrams of Fig. 4 to describe the experimental observations. In the following we shall mark the pump and scattered waves by the subscripts p and s, and ordinary and extraordinary polarization by the superscripts o and e.

When the pump waves are ordinarily polarized, parametric amplification occurs as follows (Fig. 4a): The incident pump wave with $\mathbf{k}^o_{p1}$ and the scattered wave with $\mathbf{k}^o_{s1}$ record the grating with $\mathbf{K}_2$. The second incident pump wave $\mathbf{k}^o_{p2}$ is diffracted from this grating to enhance the scattered wave $\mathbf{k}^e_{s2}$. Then $\mathbf{k}^e_{s2}$ is diffracted from the strong grating $\mathbf{K}_1$, recorded by the two pump waves, into $\mathbf{k}^o_{s1}$. Because of the $\pi/2$-phase shift of the gratings with respect to the interference pattern, there is no phase shift between the initially scattered wave $\mathbf{k}^o_{s1}$ and the wave diffracted twice, resulting from $\mathbf{k}^o_{p2} \rightarrow \mathbf{k}^e_{s2} \rightarrow \mathbf{k}^o_{s1}$ (see Section. 2.2.1).

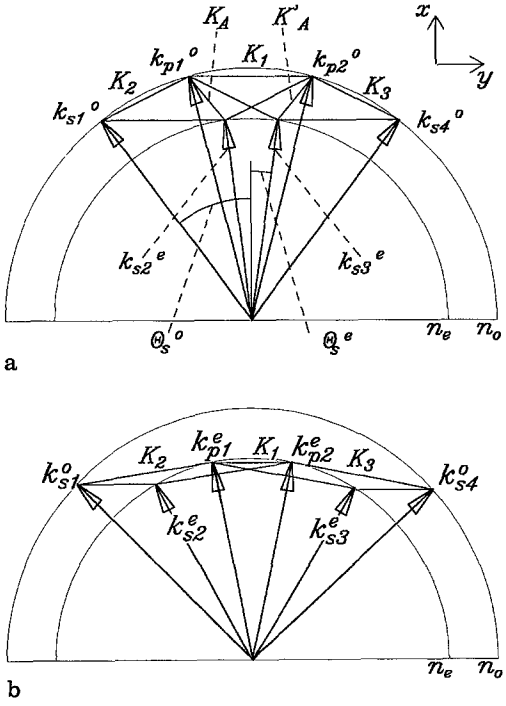

Fig. 4a, b. Phase-matching conditions in the space of wave vectors for (**a**) ordinarily and (**b**) extraordinarily polarized pump beams. The subscripts p and s denote pump and scattered waves, and the superscripts o and e ordinary and extraordinary polarization

This leads to a constructive interference and amplification of $\mathbf{k}^o_{s1}$. In this way the four waves $\mathbf{k}^o_{p1}$, $\mathbf{k}^o_{p2}$, $\mathbf{k}^o_{s1}$ and $\mathbf{k}^e_{s2}$ are coupled parametrically. Analogously, the four waves $\mathbf{k}^o_{p1}$, $\mathbf{k}^o_{p2}$, $\mathbf{k}^e_{s3}$ and $\mathbf{k}^o_{s4}$ are coupled via the gratings $\mathbf{K}_1$ and $\mathbf{K}_3$. Anisotropically written gratings, e.g., $\mathbf{K}_A$ or $\mathbf{K}'_A$ in Fig. 4a, are not considered in our model as mentioned at the beginning of this section.

For extraordinary pump wave polarization no parametric amplification can occur (Fig. 4b): In this case the incident pump wave $\mathbf{k}^e_{p2}$ and the scattered wave with $\mathbf{k}^e_{s2}$ record the grating with $\mathbf{K}_2$. The other incident pump wave $\mathbf{k}^e_{p1}$ is diffracted from this grating to enhance the scattered wave $\mathbf{k}^o_{s1}$. Then $\mathbf{k}^o_{s1}$ is diffracted from the strong grating $\mathbf{K}_1$, recorded by the two pump waves, into $\mathbf{k}^e_{s2}$. In contrast to ordinarily polarized pump waves the wave diffracted twice, resulting from $\mathbf{k}^e_{p1} \rightarrow \mathbf{k}^o_{s1} \rightarrow \mathbf{k}^e_{s2}$, is phase shifted by π with respect to the initially scattered wave $\mathbf{k}^e_{s2}$ (see Sect. 2.2.2). This results in a destructive interference and attenuation of $\mathbf{k}^e_{s2}$. For this reason dark inner lines are observed in the scattered noise (see Fig. 2b).

To check our model we calculate the dependence of the scattering angles θ^e_s and θ^o_s (in air) of the inner and outer lines in the plane of incidence (Fig. 4) from (1b). We obtain

$$\theta^e_s = \arcsin\left(\sin\theta_p - \frac{n_o^2 - n_e^2}{4\sin\theta_p}\right),$$
$$\theta^o_s = \arcsin\left(\sin\theta_p + \frac{n_o^2 - n_e^2}{4\sin\theta_p}\right), \tag{2}$$

where n_o, n_e are the refractive indices of the ordinary and extraordinary waves, respectively. In addition, we use (1b) to calculate the deviations from the straight lines for the outer and inner lines. Considering refraction at the output face of the sample and the fact that the extraordinary refractive index $n_e(\phi)$ decreases when the azimuth angle ϕ (see Fig. 1) increases, we obtain the relations

$$\left(\frac{\rho}{\rho_0}\right)^e = \frac{\cot\theta^e_s(\varphi = 0)}{\sqrt{\left[\frac{4\sin\theta_p\cos\varphi}{4\sin^2\theta_p - n_o^2 + n_e^2(\varphi)}\right]^2 - 1}}$$
$$\left(\frac{\rho}{\rho_0}\right)^o = \frac{\cot\theta^o_s(\varphi = 0)}{\sqrt{\left[\frac{4\sin\theta_p\cos\varphi}{4\sin^2\theta_p + n_o^2 - n_e^2(\varphi)}\right]^2 - 1}} \tag{3}$$

for the inner (e) and outer (o) scattering lines, respectively.

The solid lines in Fig. 3a and b represent the relations calculated from (2) and (3) with the values $n_o = 2.491$ and $n_e = 2.425$ [16]. Good agreement with the experimentally determined dependences in obvious and confirms our model. Equations (2) and (3) are valid for ordinary as well as for extraordinarily polarized pump beams. For the smallest possible grating vector $\mathbf{K}_1$, $|\mathbf{K}_1| = \Delta n = n_o - n_e = 2\sin\theta_{p,\,min}$ (Fig. 4), we find the minimum pump angle $\theta_{p,\,min} = 2°$. For smaller pump angles the phase-matching conditions cannot be fulfilled at $\lambda = 514.5$ nm in $BaTiO_3$. Furthermore, the outer and inner scattering lines cannot be observed outside the crystal because of total internal reflection at the outputface of the sample for pump angles θ_p smaller than 5° and 4.5°, respectively.

2.2 Coupled wave equations

The calculation of the output intensities and phases of the scattered waves is based on the solution of the set of coupled wave equations for slowly varying complex amplitudes A_{s1}, A_{s2}, A_{p1} and A_{p2} of the four interacting waves. This technique is widely used in nonlinear optics and also well adapted for photorefractive materials (see, e.g., [4]). If the intensity of the scattered light is small in comparison to the intensity of the pump beams, the undepleted pump approximation ($\partial A_{p1}/\partial x = 0$, $\partial A_{p2}/\partial x = 0$) may be used and the set of four equations will reduce to only two equations for the amplitudes A_{s1} and A_{s2}. One should also keep in mind that the photorefractive nonlinearity is strongly degenerate in frequency.

2.2.1 Ordinary pump wave polarization. For ordinarily polarized pump waves we derive the following set of equations:

$$\frac{\partial A_{s1}}{\partial x} = \frac{\kappa}{I_0 \cos\theta^e_{s,in}} B_{12} A_{s2},$$

$$\frac{\partial A_{s2}}{\partial x} = \frac{\kappa}{I_0 \cos\theta^e_{s,in}} B_{21} A_{s1} \tag{4}$$

with

$$B_{12} = (\mathbf{E}_{diff,1} \cdot \mathbf{e}_{s1})(\mathbf{e}_{p1} \cdot \mathbf{e}_{p2}) A_{p1} A^*_{p2},$$

$$B_{21} = -(\mathbf{E}_{diff,1} \cdot \mathbf{e}_{s1})(\mathbf{e}_{p1} \cdot \mathbf{e}_{p2}) A^*_{p1} A_{p2} + (\mathbf{E}_{diff,2} \cdot \mathbf{e}_{p2})(\mathbf{e}_{p1} \cdot \mathbf{e}_{s1}) A^*_{p1} A_{p2}. \tag{5}$$

Here $I_0 = |A_{p1}|^2 + |A_{p2}|^2$ is the total intensity of the pump waves, $\kappa = \pi n_0^2 n_e r_{131}/\lambda$ the coupling constant, r_{131} the electrooptic coefficient involved, $\mathbf{e}_{p1}$, $\mathbf{e}_{p2}$, $\mathbf{e}_{s1}$, $\mathbf{e}_{s2}$ are the polarization unit vectors of the pump and scattered waves and $\mathbf{E}_{diff,1}$, $\mathbf{E}_{diff,2}$ the diffusion fields for the gratings with the wave vectors $\mathbf{K}_1$ and $\mathbf{K}_2$:

$$\mathbf{E}_{diff,1} = \frac{k_B T}{e} \frac{\mathbf{K}_1}{1 + |\mathbf{K}_1|^2/K_s^2}$$

$$\mathbf{E}_{diff,2} = \frac{k_B T}{e} \frac{\mathbf{K}_2}{1 + |\mathbf{K}_2|^2/K_s^2} \tag{6}$$

where k_B denotes the Boltzmann constant. T the absolute temperature, $K_s = \sqrt{e^2 N_{eff}/\varepsilon\varepsilon_0 k_B T}$ the Debeye screening factor, e the absolute value of electron charge and N_{eff} the effective number of traps. The subscript in stands for angles inside the sample. By using the boundary conditions $A_{s1}(x=0) = A_{s10}$ and $A_{s2}(x=0) = A_{s20}$ we develop solution for the amplitudes of the scattered waves in the steady state:

$$A_{s1} = A_{s10}\cosh(\Gamma x) + A_{s20}\sqrt{\frac{B_{12}}{B_{21}}}\sinh(\Gamma x)$$

$$A_{s2} = A_{s20}\cosh(\Gamma x) + A_{s10}\sqrt{\frac{B_{21}}{B_{12}}}\sinh(\Gamma x) \tag{7}$$

with the gain factor

$$\Gamma = \frac{\kappa}{I_0 \cos\theta^e_{s,in}} \sqrt{B_{12} B_{21}}. \tag{8}$$

The expression under the square root is real and the gain factor Γ is purely imaginary or real. For large real gain ($\Gamma x \gg 1$) the scattered light is amplified exponentially. For imaginary gain $\Gamma = i|\Gamma|$ the hyperbolic functions in (7) become trigonometric ($\sin|\Gamma|x$, $\cos|\Gamma|x$). No steady-state amplification occurs in this case, only the phases of the transmitted seed waves change with increasing $|\Gamma|x$.

For real gain and exponential amplification the inequality $B_{12}B_{21} > 0$ has to be fulfilled. This can be written as

$$|\mathbf{E}_{diff,1}| < |\mathbf{E}_{diff,2}|. \tag{9}$$

From (6) one can see that this inequality strongly depends on the pump angle θ_p and the effective number N_{eff} of traps. Equal diffusion fields are obtained for $|\mathbf{K}_1| = |\mathbf{K}_2|$ which yields the pump angle $\theta_p = 12°$, independent of N_{eff}. Figure 5 shows the calculated dependences of the gain factor Γ on the pump angle θ_p and the effective trap number N_{eff}. Note that for $N_{eff} > 13.5 \times 10^{22}\,m^{-3}$ exponential amplification is possible only for pump angles $\theta_p < 12°$, whereas for $N_{eff} < 13.5 \times 10^{22}\,m^{-3}$ exponential amplification can be observed only for $\theta_p > 12°$. For $\theta_p > 12°$ and $N_{eff} < 13.5 \times 10^{22}\,m^{-3}$ the gain factor Γ increases with decreasing N_{eff} because of increasing difference $|\mathbf{E}_{diff,2}| - |\mathbf{E}_{diff,1}|$, and decreases because of decreasing $|\mathbf{E}_{diff,1}|$. This leads to a maximum of Γ for $N_{eff} = 7 \times 10^{22}\,m^{-3}$.

The steady-state intensities of the scattered wave for $e^{\Gamma x} \gg 1$ and $A_{s10} \gg A_{s20}$ read:

$$|A_{s1}|^2 = \tfrac{1}{4}|A_{s10}|^2 e^{2\Gamma x},$$

$$|A_{s2}|^2 = \tfrac{1}{4}|A_{s10}|^2 e^{2\Gamma x}|B_{21}/B_{12}|. \tag{10}$$

2.2.2 Extraordinary pump wave polarization. For extraordinarily polarized pump waves we obtain the same set of equations (4) (previous subsection) as for ordinarily polarized pump waves, but with different factors:

$$B_{12} = (\mathbf{E}_{diff,1} \cdot \mathbf{e}_{s1} + \mathbf{E}_{diff,2} \cdot \mathbf{e}_{s1})(\mathbf{e}_{p1} \cdot \mathbf{e}_{s1}) A_{p1} A^*_{p2},$$

$$B_{21} = (\mathbf{E}_{diff,1} \cdot \mathbf{e}_{s1}) A^*_{p1} A_{p2}. \tag{11}$$

The important result is that the inequality for exponential amplification, $B_{12}B_{21} > 0$, cannot be fulfilled under any

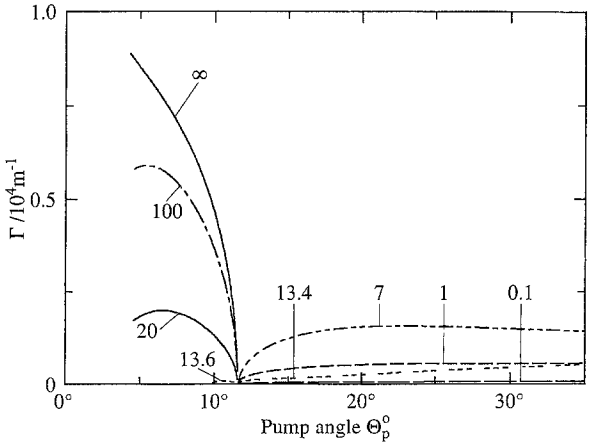

Fig. 5. Calculated gain factor Γ versus pump angle θ_p for various effective trap densities N_{eff} according to (8). The numbers are the values of $N_{eff}/10^{22}\,m^{-3}$

conditions. No steady-state amplification occurs in this case.

3 Additional experiments

In the following we present additional experiments supporting our model. To detect the involved gratings we measure the angles for Bragg diffraction at the different wavelength $\lambda = 633$ nm (see, e.g., [17]) during continuous illumination with both pump beams of wavelength $\lambda = 514.5$ nm. If a grating with a vector $\mathbf{K}$ indeed exists in the crystal, it may be read by a wave of different wavelength. From Bragg's condition

$$\mathbf{K} = \mathbf{k}^{o}_{rd} - \mathbf{k}^{e}_{rd} \tag{12}$$

(where the subscript rd denotes reading) we can deduce relations between the pump angle θ_p and the angles θ^{o}_{rd} and θ^{e}_{rd} of the incident and diffracted readout beam. In Fig. 6 these relations for the gratings $\mathbf{K}_1$ and $\mathbf{K}_2$ are compared with the measured values. The angular dependence expected for the grating $\mathbf{K}_A$ (see Fig. 4) is also included in Fig. 6. Note that for two-step diffraction such a readout of $\mathbf{K}_A = \mathbf{K}_1 - \mathbf{K}_2$ is impossible, because the Bragg condition at the changed wavelength cannot be met simultaneously for two different grating vectors $\mathbf{K}_1$ and $\mathbf{K}_2$. Thus the result of this experiment clearly indicates the existence of the gratings with the vectors $\mathbf{K}_1$ and $\mathbf{K}_2$ in the sample, whereas we do not succeed to detect gratings with the vectors $\mathbf{K}_A$ and $\mathbf{K}'_A$.

The study of the scattering dynamics reveals a significant difference for illumination with two pump beams after total erasure of all gratings, and after the crystal is pre-illuminated with one pump beam (Fig. 7a and b). In the first case we observe the usual temporal development of the scattered light intensity as observed for other parametric scattering processes in $BaTiO_3$ (see, e.g. [4]). In the steady state the intensity of the outer scattering line ($\mathbf{k}^{o}_{s1}$) is nearly two times higher than the intensity of the inner scattering line ($\mathbf{k}^{e}_{s2}$). This experimental result is well described by the ratio $I_{s2}/I_{s1} = |B_{21}/B_{12}| = 2$, which follows from (10) and (5) for a pump angle $\theta_p = 16°$ and a crystal with an effective trap number $N_{eff} = 4 \times 10^{22}\ m^{-3}$. Switching on the second pump beam $\mathbf{k}^{o}_{p2}$ after pre-illumination of the sample with only pump beam $\mathbf{k}^{o}_{p1}$, we observe a different behaviour of the light scattered into the inner line $\mathbf{k}^{e}_{s2}$, whereas the light scattered into the other lines ($\mathbf{k}^{o}_{s1}$, $\mathbf{k}^{e}_{s3}$, $\mathbf{k}^{o}_{s4}$) shows the same time dependence as

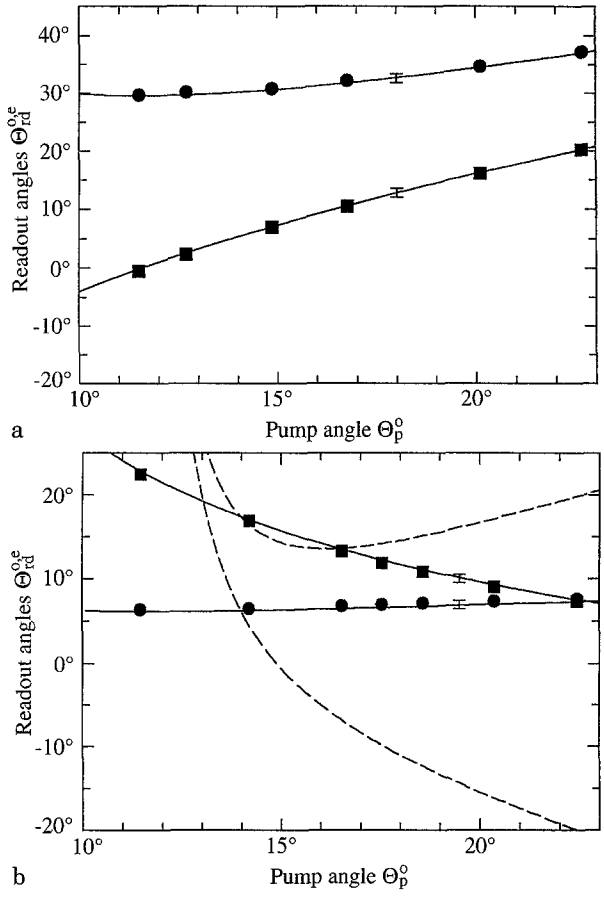

Fig. 6a, b. Dependences of the anisotropic readout angles $\theta^{o,e}_{rd}$ on the pump angle θ_p (readout wavelength $\lambda = 633$ nm, pump wavelength $\lambda = 514.5$ nm) for the gratings (**a**) $\mathbf{K}_1$ and (**b**) $\mathbf{K}_2$. The full lines represent the calculated dependences; the squares and the dots are the experimental values. The dashed lines in (**b**) are calculated for the anisotropically written grating $\mathbf{K}_A$ (see also Fig. 4a)

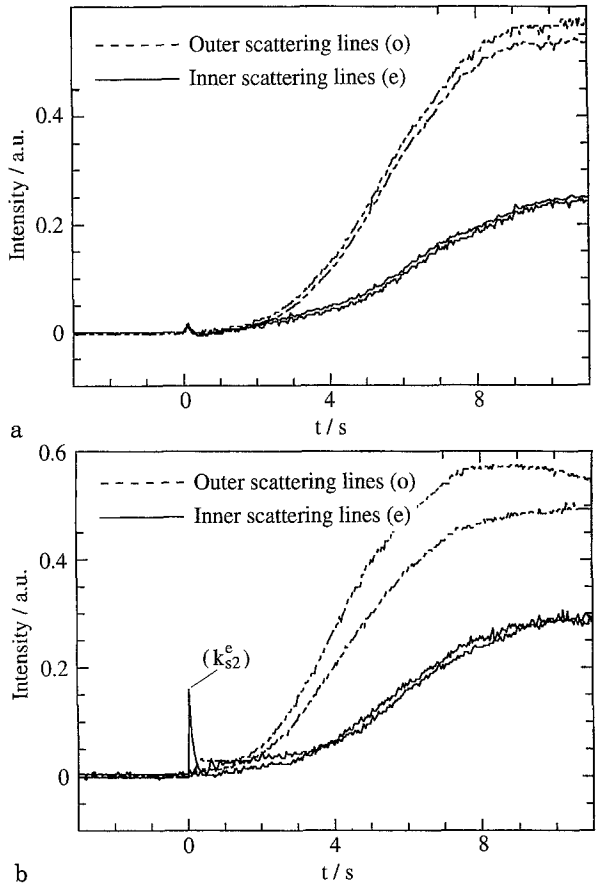

Fig. 7a, b. Temporal dependences of the intensity of the light scattered into the inner and outer lines (**a**) after all gratings were erased and (**b**) after the crystal was pre-illuminated with the pump beam $\mathbf{k}^{o}_{p1}$. At $t = 0$ s the two pump beams are switched on

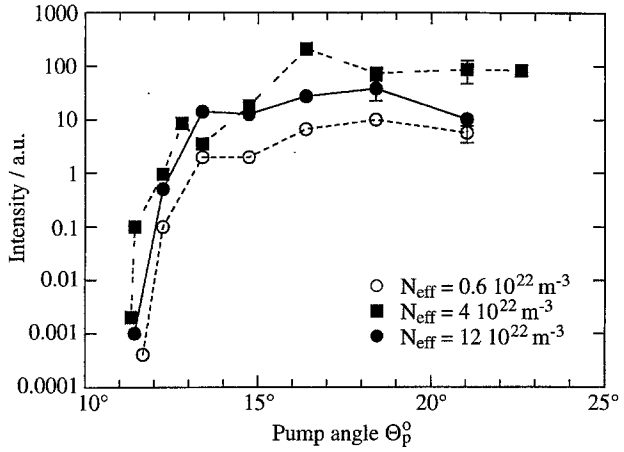

Fig. 8. Intensity (arbitrary units) of the light scattered into the inner lines as a function of the pump angle θ_p. The measurements are performed using three $BaTiO_3$ crystals with different effective trap numbers N_{eff} given in the figure. The solid and dashed curves are guides to the eye

described above (Fig. 7b). For the line $\mathbf{k}^e_{s2}$ a sharp transient peak of scattered intensity appears, followed by the usual temporal behaviour. When only the pump beam $\mathbf{k}^o_{p1}$ impinges upon the sample, it records the grating $\mathbf{K}_2$ with the initially scattered wave $\mathbf{k}^o_{s1}$ and the grating $\mathbf{K}_1$ with a wave scattered into the direction of the pump beam $\mathbf{k}^o_{p2}$. For this reason the phase of the grating $\mathbf{K}_1$ is different compared to the case of two incident pump waves. When the second pump beam $\mathbf{k}^o_{p2}$ is switched on, this beam is diffracted from the grating $\mathbf{K}_2$ and causes the strong transient peak in Fig. 7b. At the same time the grating $\mathbf{K}_1$ is overwritten with a different phase by the intensive pump beams. The increase of $\mathbf{K}_1$ diminishes the wave $\mathbf{k}^e_{s2}$, because this wave is diffracted into $\mathbf{k}^o_{s1}$. Then the usual behaviour of scattered intensity arises.

In further experiments we measure the intensity scattered into the inner line $\mathbf{k}^e_{s2}$ as a function of the pump angle for different N_{eff} values. To vary N_{eff} we use different $BaTiO_3$ crystals. The values of N_{eff} are determined by beam coupling experiments and given in Fig. 8. The scattered intensity is qualitatively well described by the calculations (see also Fig. 5). For all used crystals exponential amplification is observed only for pump angles $\theta^o_p > 12°$ (in air), in agreement with the results of chapter 2b.

4 Summary and conclusions

We investigate parametric scattering processes in $BaTiO_3$ pumped by two coherent copropagating waves. Four lines are observed on a screen behind the sample. The results of our model describe the experimental data given in the Sects. 1 and 3. First, the polarization and geometric properties of the scattering lines observed experimentally agree very well with the predictions. In addition, the necessary gratings $\mathbf{K}_1$ and $\mathbf{K}_2$ are present in the crystal, whereas no anisotropically written gratings $\mathbf{K}_A$ or $\mathbf{K}'_A$ are detected. This supports that diffusion is mainly responsible for the light-induced charge transport.

Taking into account the effective trap number N_{eff} we can explain further experimental observations:

- In the steady state the scattering lines are observed only for pump angle $\theta_p > 12°$.
- The intensity of the scattering lines increases with increasing θ_p and remains approximately constant for $\theta_p > 15°$ (see Figs. 5 and 8, $N_{eff} < 13 \times 10^{22}\ m^{-3}$).
- The intensity of the outer scattering lines may exceed the intensity of the inner scattering lines. The observed intensity ratio $I_{s2}/I_{s1} \equiv I_{s3}/I_{s4}$ is in agreement with (10).

Finally, no parametric amplification is observed for extraordinarily polarized pump waves as predicted by our model.

A similar scattering process meeting the same phase-matching conditions (1b) has been discovered earlier in $LiNbO_3$: Fe [8]. But in this case the gratings are recorded by photovoltaic charge transport yielding a different exponential gain factor. Furthermore, only the inner lines are observed.

Finally we want to emphazise that the considered parametric mixing process of four copropagating waves can be used for efficient amplification of any ordinary input wave obeying the phase-matching conditions (1b) and also for the generation of an orthogonally polarized extraordinary replica of the ordinary input wave.

Acknowledgement. We thank H. Hesse and C. Kuper for supplying the single domain $BaTiO_3$ crystals and S. Odoulov and B. Sturman for stimulating discussions. Financial support of the Deutsche Forschungsgemeinschaft (SFB 225, D9) is gratefully acknowledged.

References

1. R.A. Rupp, F.W. Drees: Appl. Phys. B **39**, 223 (1986)
2. D.A. Temple, C. Warde: J. Opt. Soc. Am. B **3**, 337 (1986)
3. M. Ewbank, P. Yeh, J. Feinberg: Opt. Commun. **59**, 423 (1986)
4. S. Odoulov, B. Sturman, L. Holtmann, E. Krätzig: Appl. Phys. B **52**, 317 (1991)
5. M. Horowitz, B. Fisher: Opt. Lett. **17**, 1082 (1992)
6. M. Goulkov, S. Odoulov, U. van Olfen, E. Krätzig: Phys. Status Solidi (b) **172**, K37 (1992)
7. B. Sturman, M. Goulkov, S. Odoulov: Appl. Phys. B **56**, 193 (1993)
8. M. Goulkov, S. Odoulov, B. Sturman: Appl. Phys. B **56**, 223 (1993)
9. J.J. Amodei, D.L. Staebler: J. Appl. Phys. **43**, 1043 (1972)
10. A. Yariv, D. Pepper: Opt. Lett. **1**, 16 (1977)
11. M. Cronin-Golomb, B. Fisher, J.O. White, A. Yariv: IEEE J. QE.-**20**, 12 (1984)
12. B. Sturman, M. Goulkov, S. Odoulov: J. Opt. Soc. Am. B (to be published)
13. J. Neumann, G. Jäkel, E. Krätzig: Opt. Lett. **20**, 1531 (1995)
14. J. Feinberg, D. Heiman, A. R. Tanguay, Jr. R. W. Hellwarth: J. Appl. Phys. **51**, 1297 (1980)
15. M. Zgonik, P. Bernasconi, M. Duelli, R. Schlesser, P. Günter, M. H. Garrett, D. Rytz, Y. Zhu, X. Wu: Phys. Rev. B **50**, 5941 (1994)
16. K. Buse, S. Riehemann, S. Loheide, H. Hesse, F. Mersch, E. Krätzig: Phys. Status Solidi (a) **135**, K87 (1993)
17. L. Holtmann, E. Krätzig, S. Odoulov: Appl. Phys. B **53**, 1 (1991)